Supporting information

p-p Heterojunction Sensors of *p*-$Cu_3Mo_2O_9$ Micro/Nanorods Vertically Grown on *p*-CuO Layers for Room Temperature Ultrasensitive and Fast-Recoverable Detection of NO_2

Bala Ismail Adamu[a,b], Attia Falak[a,b,c], Yi Tian[a], Xinghua Tan[a], Xiangmin Meng[d], Peipei Chen[a,b,], Hanfu Wang[a,*], Weiguo Chu[a,b,*]*

[a] Nanofabrication Laboratory, CAS Center for Excellence in Nanoscience, National Center for Nanoscience and Technology, Beijing 100190, China

[b] Center of Materials Science and Optoelectronics Engineering, University of Chinese Academy of Sciences, Beijing 100039, China

[c]Department of Physics, University of the Punjab, Quaid- e- Azam Campus Lahore 54000, Pakistan

[d] Technical Institute of Physics & Chemistry, Key Laboratory of Photochemical Conversion & Optoelectronic Materials, Beijing 100190, P. R. China

Email: wgchu@nanoctr.cn; chenpp@nanoctr.cn; wanghf@nanoctr.cn

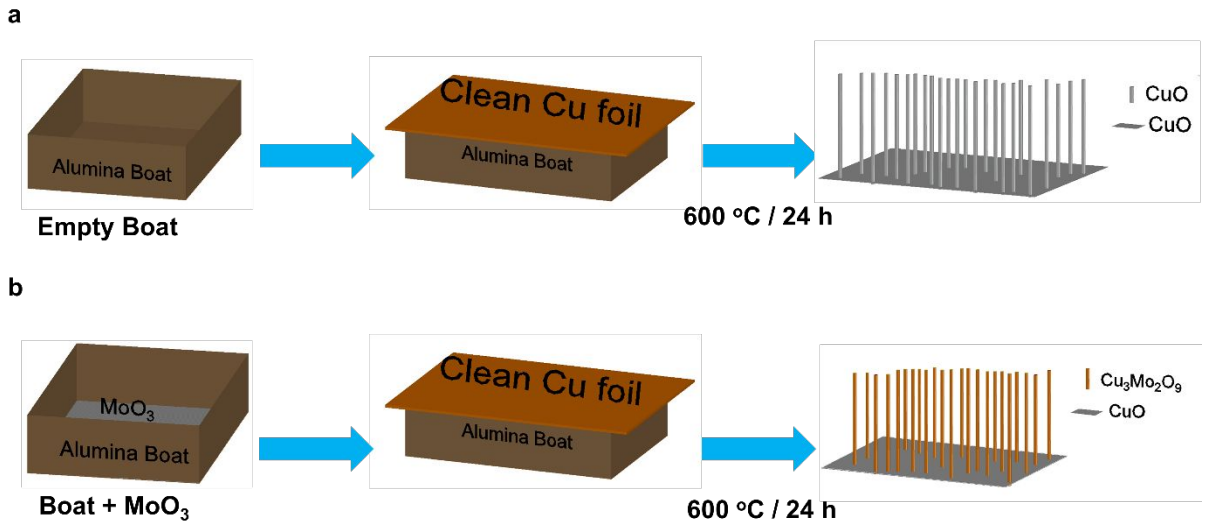

Figure S1. Schematic design and fabrication of (a) CuO@CuO, and (b) $Cu_3Mo_2O_9$@CuO sensors.

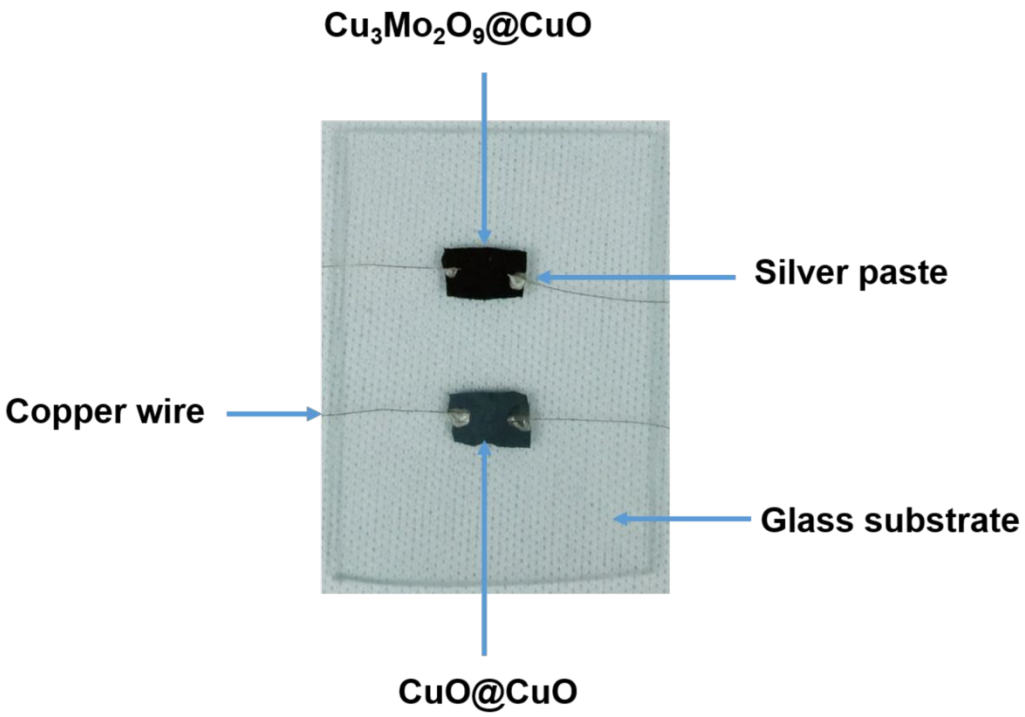

Figure S2. Photos of CuO@CuO, and $Cu_3Mo_2O_9$@CuO sensors.

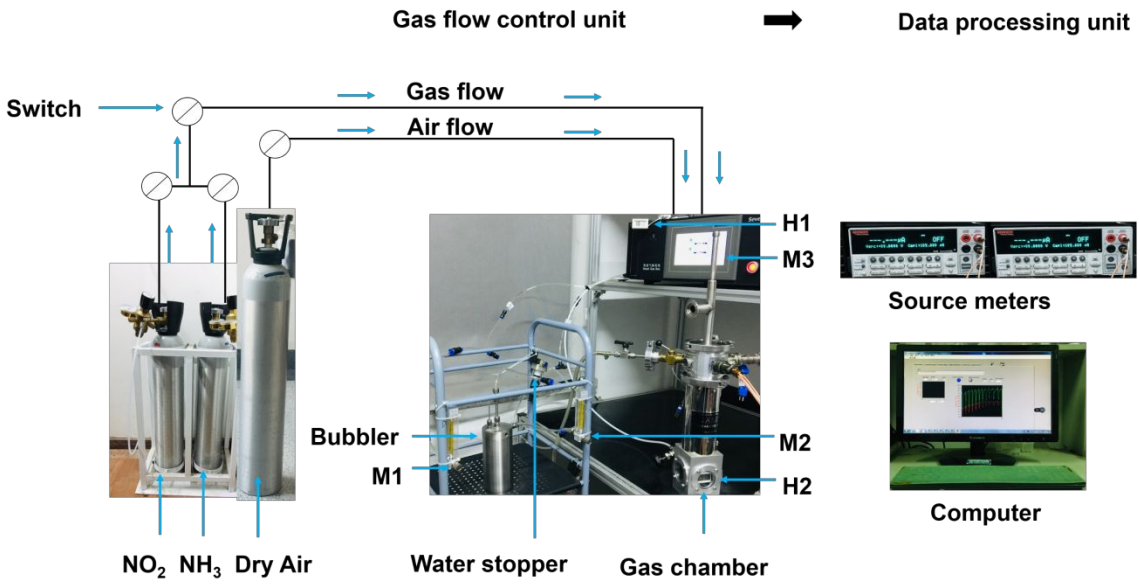

Figure S3. Gas sensing set-up.

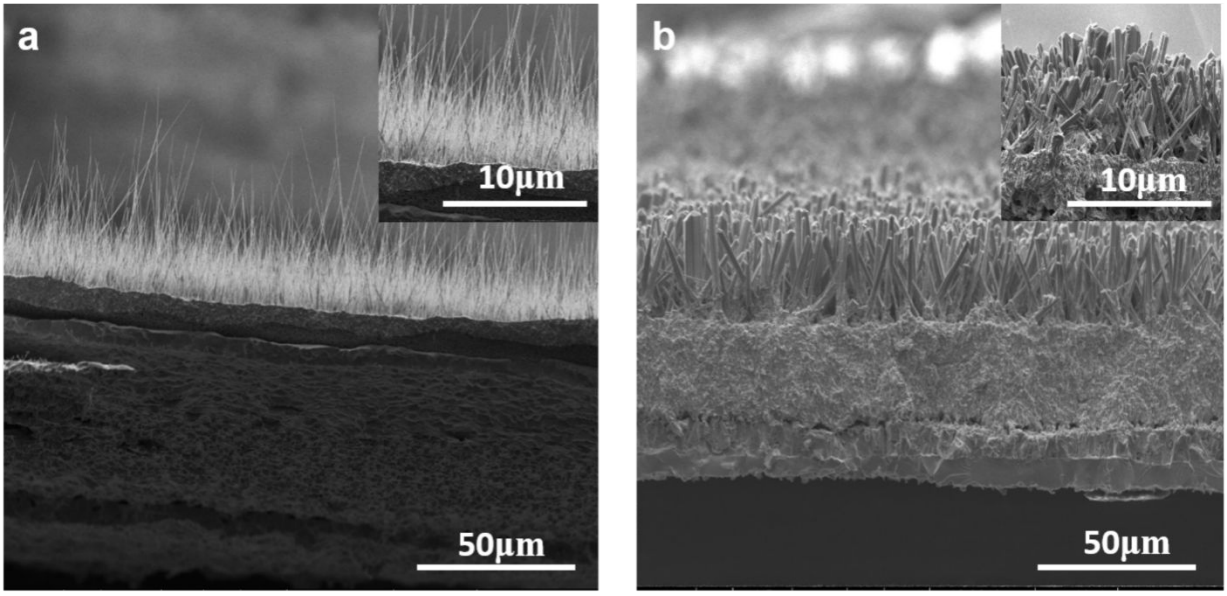

Figure S4. Side view SEM images of (a) CuO@CuO, and (b) $Cu_3Mo_2O_9$@CuO sensors.

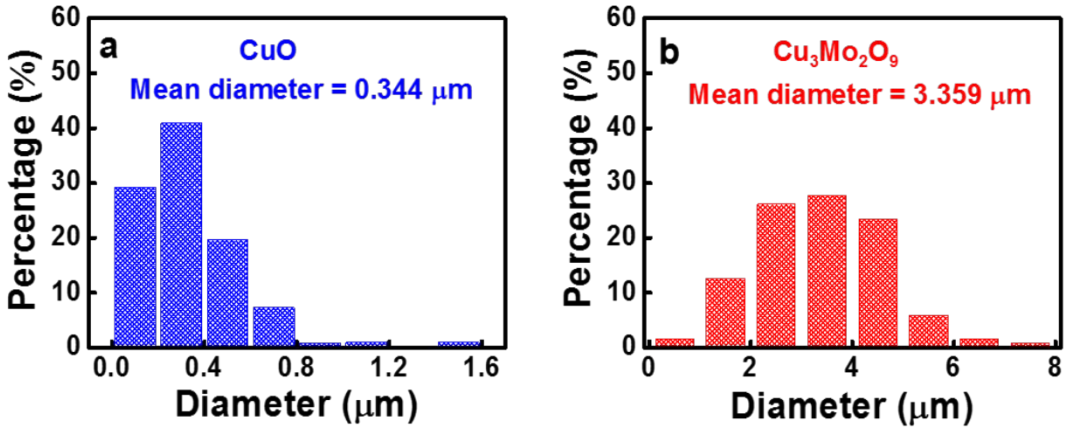

Figure S5. The diameter distribution of the nanorods in (a) CuO and (b) $Cu_3Mo_2O_9$

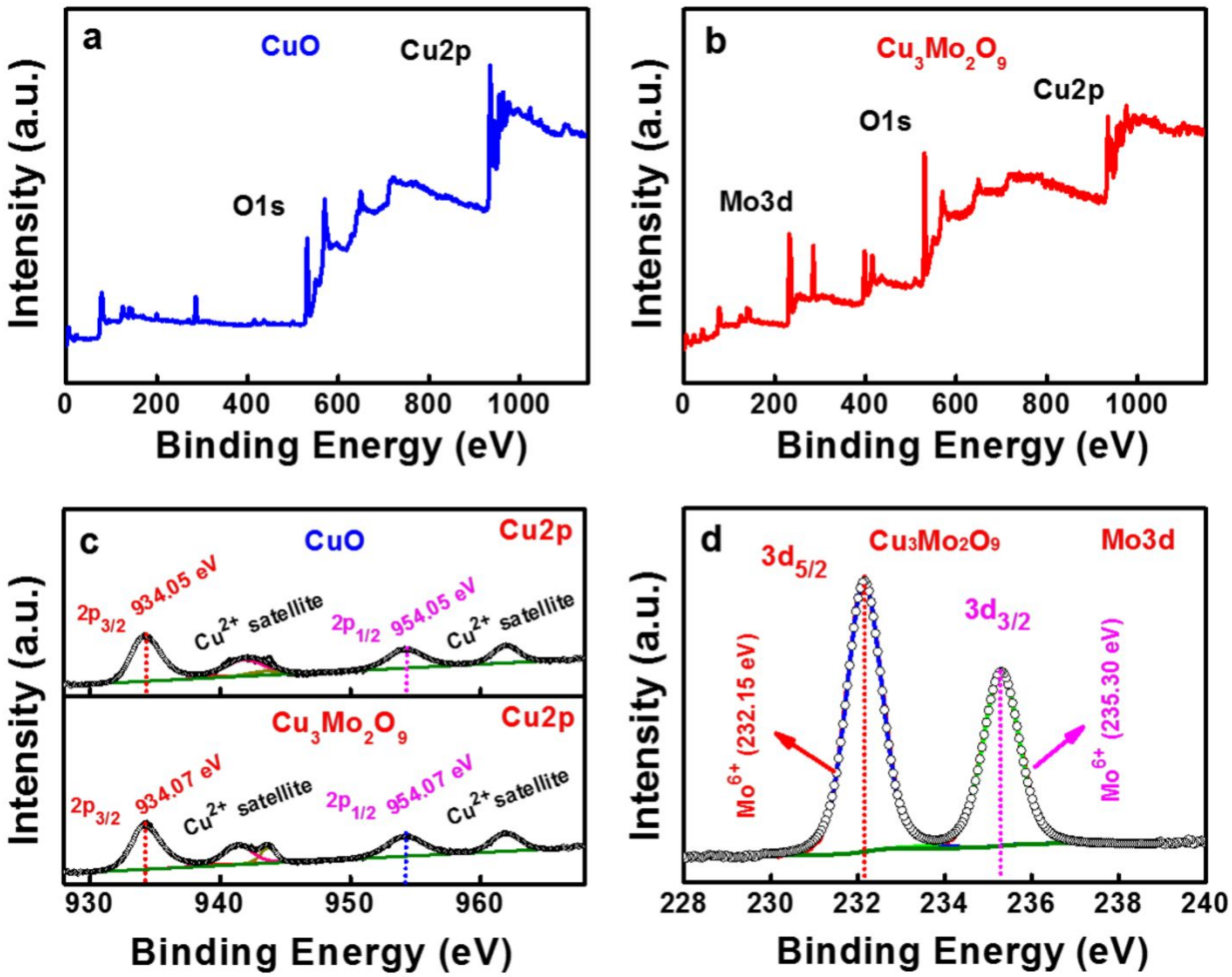

Figure S6. (a, b) Full survey-scan and (c) fine Cu2p XPS of CuO@CuO and $Cu_3Mo_2O_9$@CuO sensors, and (d) fine Mo3d spectra for $Cu_3Mo_2O_9$@CuO.

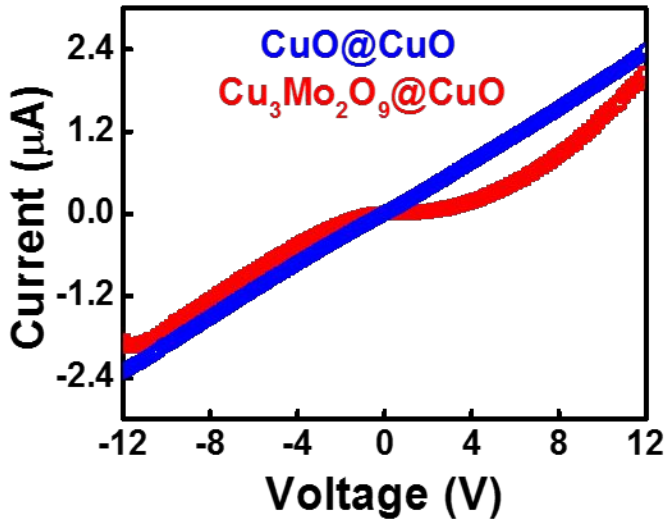

Figure S7. Comparison of *I-V* characteristics for CuO@CuO and $Cu_3Mo_2O_9$@CuO sensors at room temperature (298K).

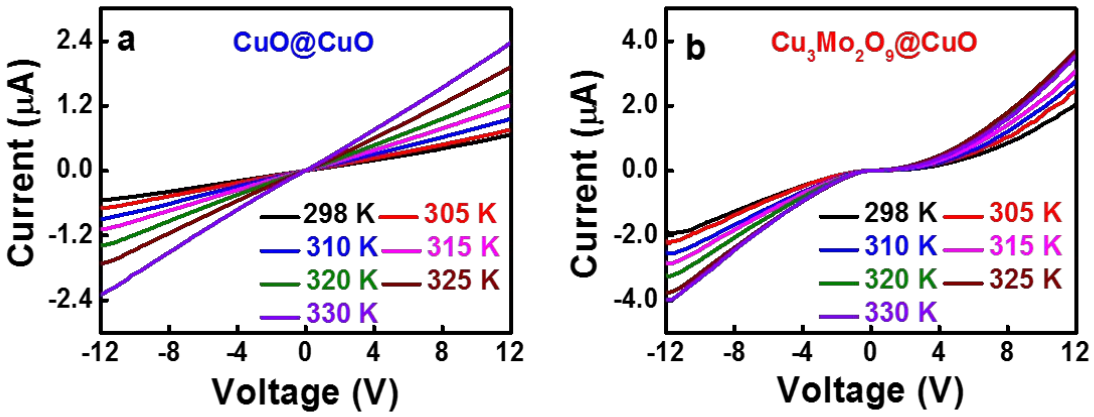

Figure S8. *I-V* characteristics curve of (a) CuO@CuO and (b) $Cu_3Mo_2O_9$@CuO sensors at various temperature (298-330 K).

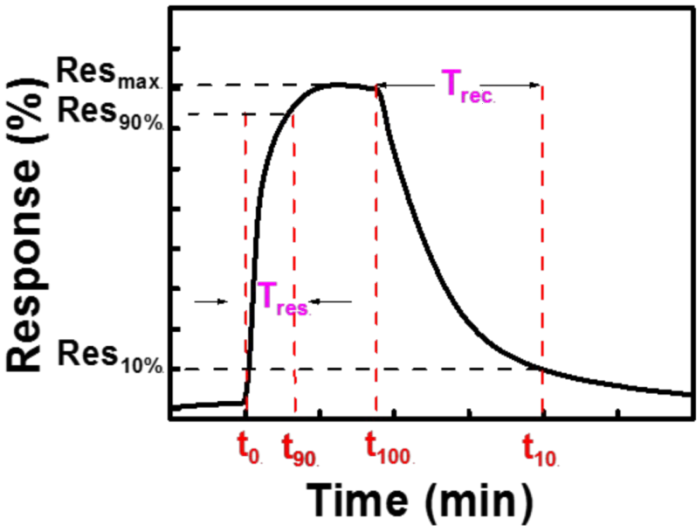

Figure S9. Method to calculate response and recovery time from dynamic gas response curve.

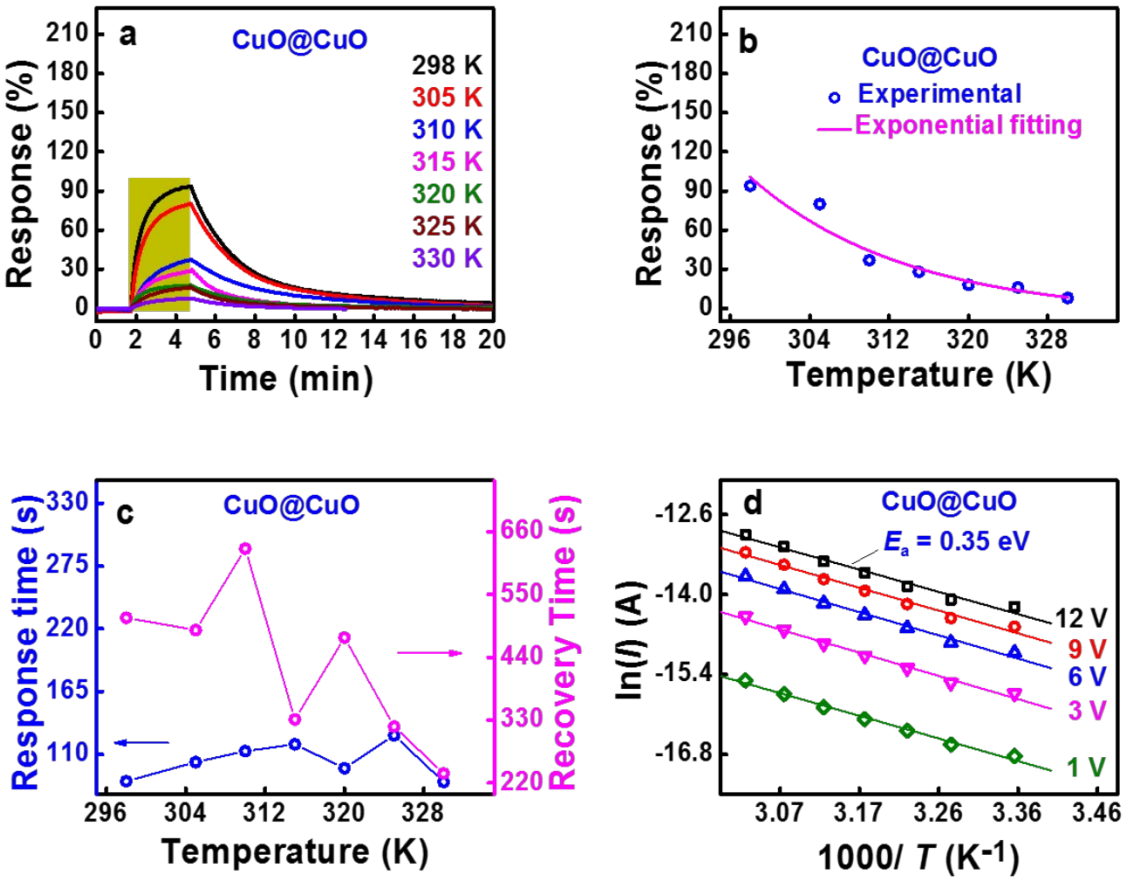

Figure S10. Temperature-dependent NO_2 gas sensing of CuO@CuO. (a) Dynamic response curves for 5 ppm NO_2 in the temperature range of 298 K-330 K, (b) Exponential decay of response with temperature, (c) Changes of response and recovery time against temperature, and (d) Relationships between logarithmic current and reciprocal temperature (Ln(*I*) versus 1/*T*) at different voltages applied from which the activation energy, E_a could be derived.

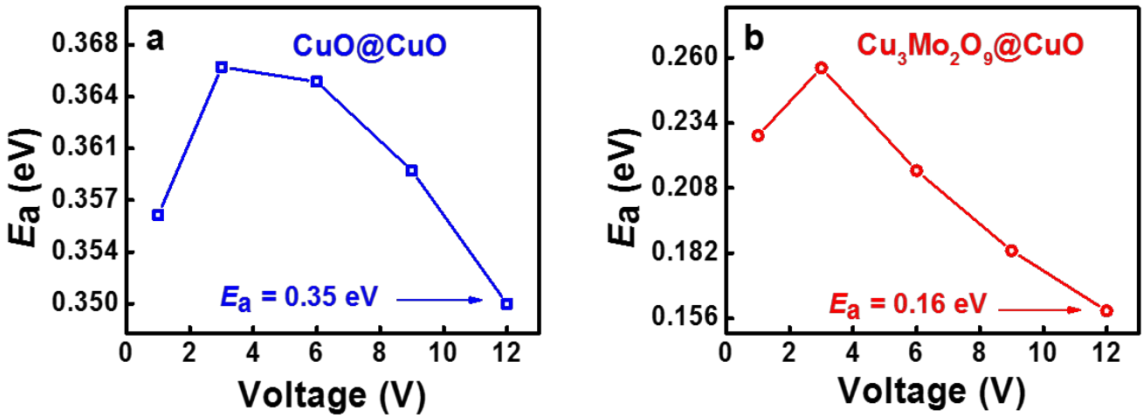

Figure S11. (a) The activation energy as a function of V_{ds} for (b) CuO@CuO sensor (c) $Cu_3Mo_2O_9$@CuO sensor.

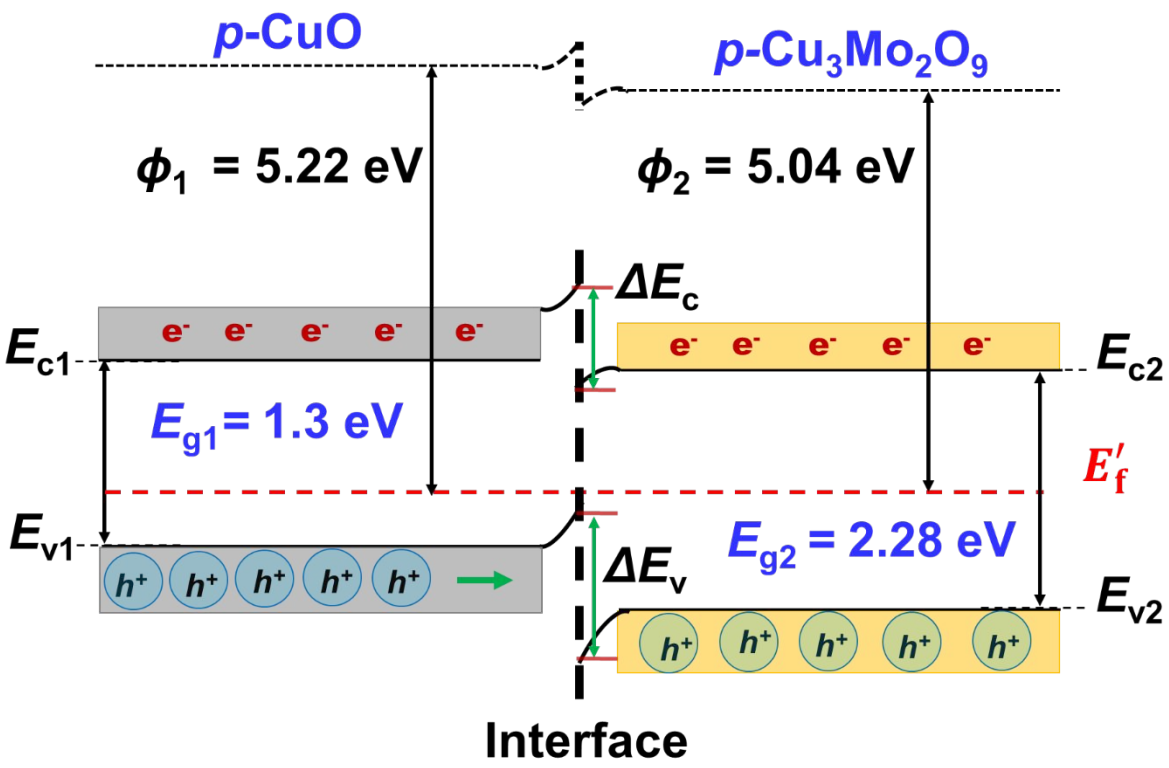

Figure S12. The energy band bending and barrier height representation with respect to E_c, E_v, E_a and E_f are conduction band, valence band, activation energy and Fermi energy respectively.

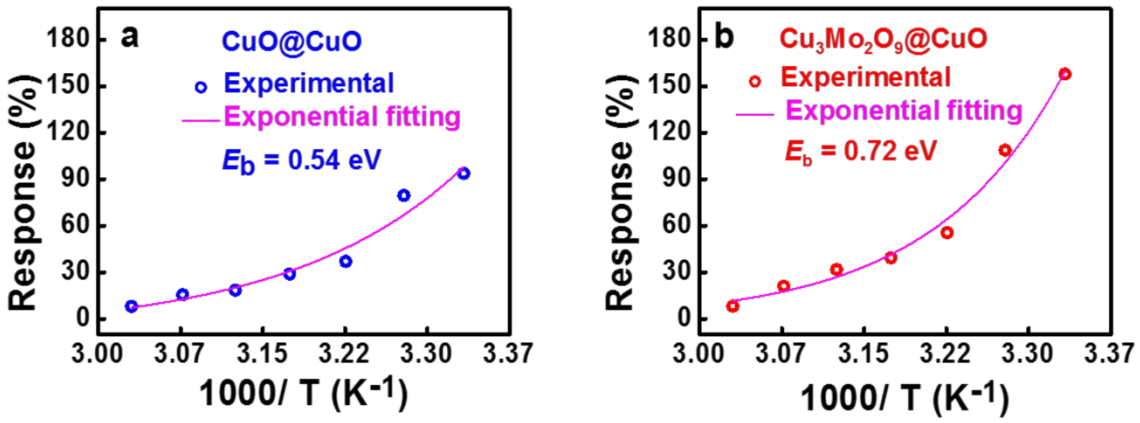

Figure S13. The Arrhenius plot used to determine adsorption energy, E_b (after exposure to NO_2) from the exponential fitting of temperature-dependent normalized response from 298-330 K for (a) CuO@CuO sensor (b) $Cu_3Mo_2O_9$@CuO sensor.

Table S1. Comparison of length, Diameter and Volume of CuO and $Cu_3Mo_2O_9$ micro/ nanorods.

CuO			$Cu_3Mo_2O_9$		
Mean Length (μm)	Mean Diameter (μm)	Mean Volume (μm^3)	Mean Length (μm)	Mean Diameter (μm)	Mean Volume (μm^3)
6.127	0.344	0.569	7.615	3.359	67.481

Table S2. Comparison of response and recovery times for CuO@CuO and $Cu_3Mo_2O_9$@CuO sensors at Room temperature (298K).

CuO@CuO			$Cu_3Mo_2O_9$@CuO		
Max	Respon	Recover	Max	Respons	Recovery

Concentration (ppm)	Response (%)	se time (sec)	y time (sec)	Response (%)	e time (sec)	time (sec)
5	94	88.8	511.2	160	49.8	241.2
4	86	83.4	498.0	136	58.8	237.6
3	80	96.0	505.2	128	70.8	265.2
2	73	109.2	544.2	114	85.2	305.4
1	60	121.2	552.6	88	73.2	382.2
0.8	52	123.6	640.8	80	81.0	427.8
0.6	44	118.8	587.4	70	90.6	472.8
0.4	38	133.2	636.0	60	115.8	556.2

Table S3. Comparison of sensitivity, RMS_{noise} and LOD for CuO@CuO and $Cu_3Mo_2O_9$@CuO in low and high concentration range 1-0.4ppm and 1-5 ppm.

Concentration region	Sensor	Sensitivity (%ppm^{-1})	R^2 for Linear Fit	RMS_{noise} (%)	LOD (ppb)
Low	CuO@CuO	33	0.9333	0.090404	8.21
	$Cu_3Mo_2O_9$@CuO	50	0.9920	0.03826	2.30
High	CuO@CuO	6.9	0.9333	0.090404	39.31
	$Cu_3Mo_2O_9$@CuO	14.46	0.9920	0.03826	7.94

Table S4. Summary of temperature-dependent activation energy barriers for CuO@CuO and $Cu_3Mo_2O_9$@CuO sensors in the voltage range 1- 12 V.

	CuO@CuO	$Cu_3Mo_2O_9$@CuO
Voltage (V)	E_a (eV)	E_a (eV)
1	0.356	0.229
3	0.366	0.256
6	0.365	0.215
9	0.359	0.183
12	0.350	0.160

Table S5. Summary of activation energy barriers after NO_2 exposure for CuO@CuO and $Cu_3Mo_2O_9$@CuO sensors at 12 V.

CuO@CuO	$Cu_3Mo_2O_9$@CuO
E_b	E_b

(eV)	(eV)
0.54	0.72

The reflection spectra of CuO@CuO and $Cu_3Mo_2O_9$@CuO micro/ nanorods were transformed into absorption spectra using the Kubelka-Munk function $\left(F(R) = \frac{(1-R)^2}{2R} = \frac{\alpha}{S}\right)$ in the wavelength range 200 nm to 800 nm. Here, *R* is reflectance, α is an absorption coefficient and *S* is the scattering coefficient. The scattering coefficient is weakly dependent on energy, therefore *K-M* function is directly proportional to the absorption coefficient, α. The Tauc equation defining a relation between the absorbance coefficient and band gap is given as Equation (1), where, *c* is proportionality constant, E_g is bandgap energy and index *n* represents a type of transitions (taking *n*= ½ for direct allowed transitions). [1,2]

$$(\alpha \times E)^n = c(E - E_g) \quad (1)$$

According to the tapping mode of AFM, Kelvin Prove Force Microscopy (KPFM) provides an effective approach to examine the surface potential difference of the thin film with high resolution. Therefore, contact potential difference (V_{CPD}) between the scanning tip (Pt) and the sample surface is defined as [3]

$$V_{CPD} = \frac{\phi_{tip} - \phi_{sample}}{e} \quad (2)$$

Here, ϕ_{sample} and ϕ_{tip} are the work functions of sample and the tip respectively; e is the electronic charge in electron volt (eV).

According to the Arrhenius equation, the current flow in the semiconducting material as a function of temperature can be represented as

$$I = I_0 e^{-\frac{E_a}{kT}} \quad (3)$$

Where K is the Boltzmann's constant. Therefore, gas response, R can be defined as

$$R = \frac{I_1 - I_o}{I_o} = \frac{I_1 e^{-\frac{E_{ad}}{kT}} - I_0 e^{-\frac{E_a}{kT}}}{I_0 e^{-\frac{E_a}{kT}}} = \frac{I_1}{I_0} e^{\left[\frac{(E_a - E_{ad})}{KT}\right]} - 1 = R_o\, e^{\left(\frac{E_b}{KT}\right)} - 1 \quad (4)$$

Where $R_o = \frac{I_1}{I_0}$, and E_{ad}, E_a and E_b are adsorption energy barrier, activation energy barrier prior to NO_2 exposure at different temperatures (which could be derived directly from equation (3)) and activation energy after NO_2 exposure respectively. Therefore, we can fit the last term of equation (4) to determine the parameters of E_b from the response vs temperature curve. Hence we can define the adsorption energy barrier based on the modified Arrhenius equation as [4]

$$E_{ad} = E_a - E_b \quad (5)$$

REFERENCES

(1) Venugopal, B.; Nandan, B.; Ayyachamy, A.; Balaji, V.; Amirthapandian, S.; Panigrahi, B. K.; Paramasivam, T. Influence of Manganese Ions in the Band Gap of Tin Oxide Nanoparticles: Structure, Microstructure and Optical Studies. *RSC Adv.* **2014**, *4*, 6141–6150.

(2) Gupta, D.; Meher, S. R.; Illyaskutty, N.; Alex, Z. C. Facile Synthesis of Cu_2O and CuO Nanoparticles and Study of Their Structural, Optical and Electronic Properties. *J. Alloys Compd.* **2018**, *743*, 737–745.

(3) Chen, Y.; Zhang, L.; Zhang, H.; Zhong, K.; Zhao, G.; Chen, G. Band Gap Manipulation and Physical Properties of Preferred Orientation CuO Thin Films with Nano Wheatear Array. *Ceram. Int.* **2018**, *44*, 1134–1141.

(4) Santra, A. K.; Min, B. K.; Yi, C. W.; Luo, K.; Choudhary, T. V.; Goodman, D. W. Decomposition of NH_3 on Ir (100): A Temperature Programmed Desorption Study.

J. Phys. Chem. B **2002**, *106*, 340–344.